analytical chemistry

pubs.acs.org/ac

Article

Rapid Screening of COVID-19 Directly from Clinical Nasopharyngeal Swabs Using the MasSpec Pen

Kyana Y. Garza,[▽] Alex Ap. Rosini Silva,[▽] Jonas R. Rosa, Michael F. Keating, Sydney C. Povilaitis, Meredith Spradlin, Pedro H. Godoy Sanches, Alexandre Varão Moura, Junier Marrero Gutierrez, John Q. Lin, Jialing Zhang, Rachel J. DeHoog, Alena Bensussan, Sunil Badal, Danilo Cardoso de Oliveira, Pedro Henrique Dias Garcia, Lisamara Dias de Oliveira Negrini, Marcia Ap. Antonio, Thiago C. Canevari, Marcos N. Eberlin, Robert Tibshirani, Livia S. Eberlin,* and Andreia M. Porcari*

Cite This: https://doi.org/10.1021/acs.analchem.1c01937

Read Online

ACCESS | Metrics & More | Article Recommendations | Supporting Information

ABSTRACT: The outbreak of COVID-19 has created an unprecedent global crisis. While the polymerase chain reaction (PCR) is the gold standard method for detecting active SARS-CoV-2 infection, alternative high-throughput diagnostic tests are of a significant value to meet universal testing demands. Here, we describe a new design of the MasSpec Pen technology integrated to electrospray ionization (ESI) for direct analysis of clinical swabs and investigate its use for COVID-19 screening. The redesigned MasSpec Pen system incorporates a disposable sampling device refined for uniform and efficient analysis of swab tips via liquid extraction directly coupled to an ESI source. Using this system, we analyzed nasopharyngeal swabs from 244 individuals including symptomatic COVID-19 positive, symptomatic negative, and asymptomatic negative individuals, enabling rapid detection of rich lipid profiles. Two statistical classifiers were generated based on the lipid information acquired. Classifier 1 was built to distinguish symptomatic PCR-positive from asymptomatic PCR-negative individuals, yielding a cross-validation accuracy of 83.5%, sensitivity of 76.6%, and specificity of 86.6%, and validation set accuracy of 89.6%, sensitivity of 100%, and specificity of 85.3%. Classifier 2 was built to distinguish symptomatic PCR-positive patients from negative individuals including symptomatic PCR-negative patients with moderate to severe symptoms and asymptomatic individuals, yielding a cross-validation accuracy of 78.4%, specificity of 77.21%, and sensitivity of 81.8%. Collectively, this study suggests that the lipid profiles detected directly from nasopharyngeal swabs using MasSpec Pen-ESI mass spectrometry (MS) allow fast (under a minute) screening of the COVID-19 disease using minimal operating steps and no specialized reagents, thus representing a promising alternative high-throughput method for screening of COVID-19.

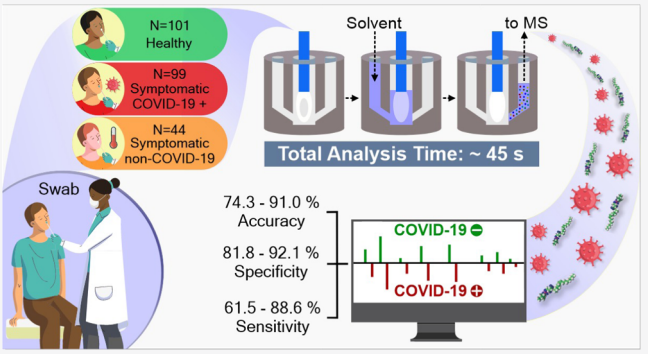

INTRODUCTION

The novel coronavirus disease 2019 (COVID-19), caused by the severe acute respiratory syndrome coronavirus 2 (SARS-CoV-2), has presented an unprecedented global challenge to society and public health.[1,2] As vaccines have yet to be widely administered to the public, especially in resource-limited countries, and their effectiveness toward new variants is yet to be determined, mitigation of disease transmission relies heavily on the widespread availability of rapid COVID-19 tests exhibiting robust analytical performance and diagnostic metrics including adequate sensitivity, specificity, and low false-positive rates (FPR) and false-negative rates (FNR).[3,4] Current diagnostic assays for COVID-19 are largely based on the detection of SARS-CoV-2 ribonucleic acid (RNA) via quantitative polymerase chain reaction (qPCR) analysis. PCR is a powerful and highly sensitive assay; yet, clinical laboratories have faced challenges in maintaining current demands due to limited availability of the specialized test reagents, instrumentation that have been overrun beyond their capabilities, and low-throughput analyses.[5] Alternative diagnostic tests that have little to no reagent requirements and provide a rapid turnaround time are highly valuable for COVID-19 detection.[6] For example, serological tests targeting host antibodies have been deployed for COVID-19 diagnosis, yielding promising results.[7,8] Yet, the inability to diagnose

Received: May 7, 2021
Accepted: August 6, 2021

early-stage or acute infections with antibody testing, along with potential cross-reactivity from prior infections by other pathogens presents a challenge for patient screening.[9] Antigen tests have been developed to rapidly identify active SARS-CoV-2 infections via the detection of the nucleocapsid protein antigen.[6] While antigen tests provide diagnosis in ∼15 min, FNR of up to 40% has been reported due to higher limits of detection compared to PCR.[10−12] Alternative testing and screening methods capable of rapidly screening for COVID-19 disease are thus still needed to increase testing capacity and throughput.

COVID-19 tests targeting molecular species other than viral RNA are currently being evaluated as rapid screening methods prior to PCR analysis to mitigate viral outbreaks. Lipids present an interesting molecular target for identifying SARS-CoV-2 infection as these molecules are a major component of the viral envelope and are involved in key replication cycle processes, including the production of new virions.[13,14] Viral genetic material does not code for lipids but sequesters these molecules from their host cellular membranes during budding. The lipid composition of the host-derived viral envelope is known to be specific to the budding site[15] and quantitatively distinct from that of the host membrane and from other viruses.[16−19] Coronaviruses, for example, bud and derive their viral envelope lipids from the membrane of the host endoplasmic reticulum (ER)-Golgi intermediate complex,[16] whereas the influenza virus acquire their lipids from the host apical plasma membrane.[20] In a study by Van Genderen et al., the proportion of phosphatidylinositol (PI) in the viral membranes of coronavirus murine hepatitis virus (MHV) was found to be elevated by 4% compared to the host cells, and the ratio of phosphatidylserine (PS) to PI species was reduced by 12%.[21] Viral pathogens also remodel host lipid metabolism to enable replication during infection, altering the overall lipid composition of infected host cells. For example, Yan et al. described that fatty acids and glycerophospholipids were significantly elevated in human cells infected with the HCoV 229E coronavirus compared to healthy cells.[22] Dysregulation of highly abundant glycerophospholipids in infected host cells and the unique lipid composition of the pathogen itself, therefore, represent a promising target for diagnostic tests.

Mass spectrometry (MS) techniques have been largely applied to study infectious diseases, targeting various biological molecules to identify bacterial and viral infections.[23−27] Recently, MS techniques have been explored to detect COVID-19 based on metabolite, lipid, and protein information.[28−34] For example, liquid chromatography MS and machine learning models have been used to identify proteomic and metabolic signatures in sera from COVID-19 patients with 93.5% accuracy for a training set of 31 samples.[31] Matrix-assisted laser desorption/ionization mass spectrometry (MALDI-MS) was also used to analyze extracts of nasal swabs[29] and plasma[35] to diagnose COVID-19. Ambient ionization MS and machine learning have been explored to detect SARS-CoV-2 infection based on fatty acid and lipid profiles.[30] De Silva et al. used paper spray MS to analyze lysed cell extracts from 30 symptomatic COVID-19 positive and symptomatic negative patients, with 93.3% agreement with PCR based on 11 metabolites, fatty acids, and lipids,[30] whereas Ford et al. used desorption electrospray ionization (DESI) and laser desorption rapid evaporative ionization mass spectrometry (LD-REIMS) to analyze 70 nasal swabs, with accuracies over 84.0%.[32] As MS technologies steadily advance toward clinical implementation, these studies showcase the potential of MS-based assays for screening and diagnosis of viral infections.

Here, we report a new design of the MasSpec Pen technology for the analysis of swabs and demonstrate its use for rapid and direct lipid analysis and potential for COVID-19 screening. We previously reported the development of the MasSpec Pen as a handheld device integrated to a mass spectrometer for direct and rapid molecular analysis of tissues.[36,37] While the handheld MasSpec Pen was designed as an easy-to-use device that enabled precise and efficient molecular analyses of sample surfaces using a solvent droplet, it precludes sufficient sampling and full area coverage of three-dimensional samples such as swab tips that contain heterogeneous adhesion and distribution of mucous secretion. To that end, we optimized the disposable device to enable uniform sampling of an entire swab tip via liquid extraction using common solvents, and thus efficient molecular extraction and analysis. The disposable sampling system was then directly integrated to an ESI source for sensitive detection of molecular ions. Using the MasSpec Pen-ESI MS system, we obtained rich lipid profiles from nasopharyngeal swabs and built statistical classification models to evaluate its prediction capabilities for COVID-19. Collectively, our study shows that direct analysis of clinical swabs with the MasSpec Pen-ESI MS technology is a promising method for rapid screening of viral infections such as COVID-19.

MATERIALS AND METHODS

Chemicals. Cardiolipin (CL) 72:4, phosphatidylglycerol (PG) 36:2, and phosphatidylethanolamine (PE) 36:2 lipid standards were purchased from Avanti Polar Lipids (Alabaster, AL). PG and PE standards were dissolved in methanol at a concentration of 10 μM, and the CL standard was dissolved in methanol at a concentration of 13 μM.

Design and Fabrication of the Adapted MasSpec Pen-ESI System. The MasSpec Pen polydimethylsiloxane (PDMS) swab sampling device was designed in CAD software and negative molds for the devices were fabricated using procedures previously described (Methods and Supporting Information).[37] The subatmospheric pressure ESI source was built by modifying the housing of a commercially available atmospheric pressure chemical ionization (APCI) source (Agilent Technologies). See the Supporting Information for details on the modifications made to the APCI source and materials used to make the lab-built sprayer.

Clinical Nasopharyngeal Swabs. Nasopharyngeal swabs from symptomatic SARS-CoV-2 PCR-positive and symptomatic and asymptomatic SARS-CoV-2 PCR-negative individuals were collected and stored in dry tubes from consented patients that were hospitalized with moderate or severe respiratory symptoms in two different hospitals (Santa Casa and Bragantino) as well as from asymptomatic volunteers at the Integrated Unit of Pharmacology and Gastroenterology (UNIFAG) in the city of Bragança Paulista (São Paulo, Brazil), by the research team at the São Francisco University (Bragança Paulista, Sao Paulo, Brazil). Approval from the Institutional Review Board (IRB) was received for the study (protocol number 31573020.9.0000.5514, approved on May 29, 2020). Viral transport media collected from SARS-CoV-2 PCR-positive and -negative patients were obtained from the Clinical Pathology Laboratories in Austin, TX. Additional details about clinical swabs and viral transport media collection, handling, and storage are given in the Supporting Information.

https://doi.org/10.1021/acs.analchem.1c01937
Anal. Chem. XXXX, XXX, XXX−XXX

Table 1. Patient Demographic Information for the Samples Used in Lasso Statistical Analysis[a]

parameters	symptomatic PCR positive	symptomatic PCR negative	asymptomatic PCR negative	p-value
Demographics				
number of patients, n	44	26	101	2.18×10^{-6}
age range, y	(21, 84)	(26, 84)	(20, 89)	
sex (female, male)	(16, 28)	(11, 15)	(58, 43)	0.0602
Symptoms				
fever	19	12		1.0000
cough	30	16		0.7602
myalgia	9	2		0.2811
sore throat	8	8		0.3590
headache	12	1		0.0342
dyspnea	29	18		0.9820
tiredness/fatigue	3	2		1.0000
loss of smell/taste	9	9		0.3045
diarrhea	11	2		0.1386
none			101	
Chest CT Features				
ground-glass opacity	42	18		0.0024
consolidations	21	14		0.8770
crazy paving appearance	21	9		0.3659
reticular pattern	6	6		0.5214
pulmonary commitment degree	37	16		0.0410
suggestive of viral infection	42	18		0.0024
Underlying Conditions				
systemic arterial hypertension	25	11	16	0.5765
cardiovascular disease	6	4	2	1.0000
obesity	10	1	22	0.0788
diabetes	16	2	3	0.0178
lung disease	4	5	8	0.3925
chronic obstructive pulmonary diesase	1	1	1	1.0000
smoker/ex-smoker	3	3	6	0.8105
asthma	2	2	2	0.9879

[a]The demographic information is for all patients and individuals included in the Lasso statistical analysis. The clinical information is for the symptomatic negative and symptomatic positive patients included in the statistical analysis.

Clinical sample collection began on July 17, 2020. Clinical diagnosis for the symptomatic patients and asymptomatic individuals was performed via reverse transcription-polymerase chain reaction (RT-PCR) analysis using a different clinical swab as part of their clinical care and independently of our study. RT-PCR was performed using the TaqPath COVID-19 RT-PCR IVD Kit (Thermo Fisher), and the results were interpreted using the COVID-19 Interpretative Software, according to the manufacturer's instructions, with a cycle threshold (Ct) value of ≤37. Table 1 provides patient demographics information. As of October 21, 2020, swabs from 268 individuals had been collected in Brazil and shipped to and received by our laboratory at UT Austin where swabs were stored at −80 °C prior to analysis.

MasSpec Pen-ESI Analysis and Data Acquisition. Prior to the analysis, the swabs were removed from the −80 °C freezer and thawed to room temperature in a class II biological safety cabinet for 15 min. To maximize safety measures, swabs were then heat-inactivated for 30 min at 65 °C. Following heat inactivation, swabs were placed in the biological safety cabinet until cooled to room temperature. Swabs were stored in a refrigerator at 4 °C until MasSpec Pen-ESI MS analysis. Swabs were analyzed within 3 days of heat inactivation.

Experiments were performed on two mass spectrometers, an LTQ-Orbitrap XL and a Q Exactive HF mass spectrometer (Thermo Fisher Scientific), in the negative ion mode. The Supporting Information provides experimental details and parameters. During MasSpec Pen-ESI MS analysis, the swab tips were inserted into the middle channel of the PDMS sampling device (Figure 1). Upon the pressing of a foot pedal, a volume of 167 μL of $CHCl_3$/MeOH was delivered from the syringe pump to the middle channel containing the swab, interacting with and extracting molecules from the swab tip for 10 s. The entire process was controlled using programmed microcontrollers. A vacuum was then applied for 30 s to the poly(tetrafluoroethylene) (PTFE) tube to enable the transport of the solvent from the swab reservoir to the ESI source. Mass spectra were acquired for ∼20−30 s.

Statistical Analysis. A total of 75 mass spectra were averaged and extracted for each sample analyzed. A mass filter of m/z 400−1000 was applied, after binning and background subtraction. Data were normalized to the TIC, and peaks appearing in less than 50% of the entire data set for each classifier were removed during cross-validation (CV). The least absolute shrinkage and selection operator (Lasso) statistical analysis was performed using the β version of the glmnet package v4.1-2, using the exclude/filtering option in glmnet. The time elapsed between PCR and MS swab collection and days since symptom onset were used as selection criteria. Swabs that were collected for MS 3 days or more after PCR sample collection and beyond 14 days of symptom onset were excluded from the classifier. From the 268 individuals who had

https://doi.org/10.1021/acs.analchem.1c01937
Anal. Chem. XXXX, XXX, XXX−XXX

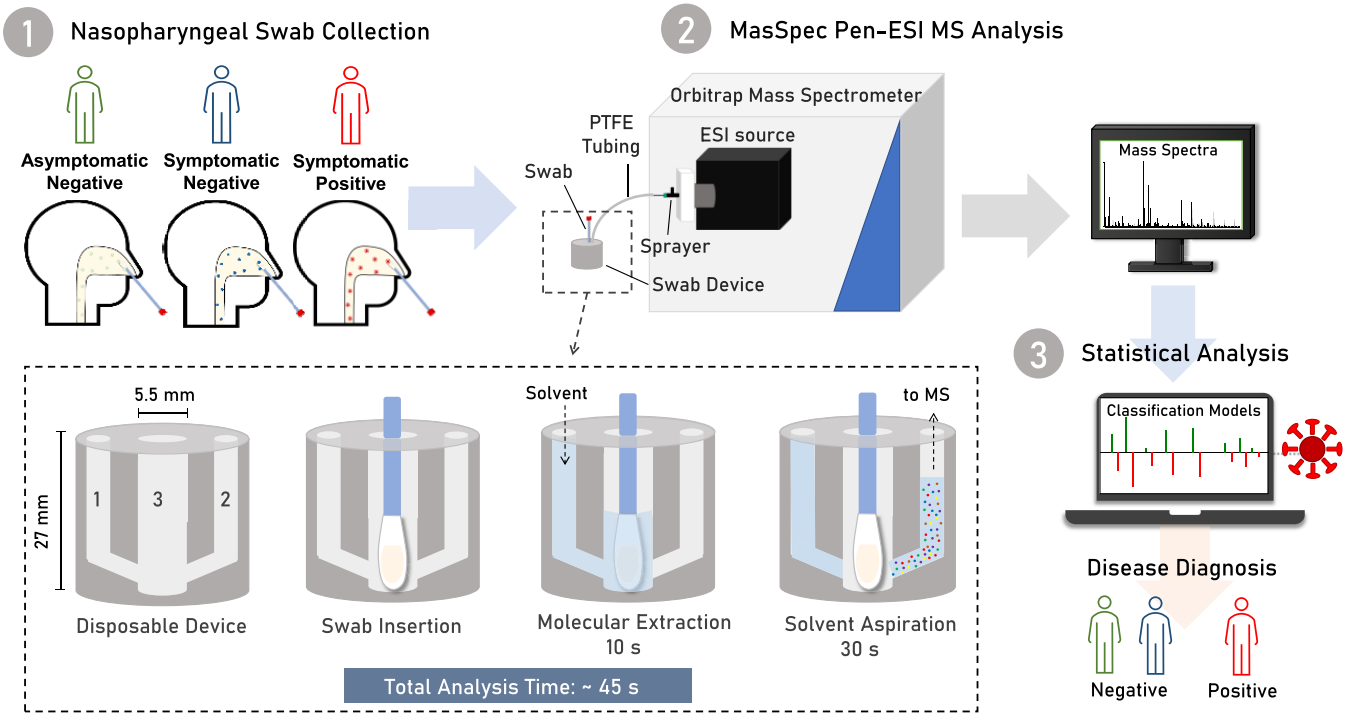

Figure 1. Schematic of the MasSpec Pen-ESI-MS system for the diagnosis of COVID-19 infection. Swabs acquired from symptomatic patients and asymptomatic individuals were analyzed by the MasSpec Pen-ESI MS platform and the mass spectra collected were used to build machine learning classification models for diagnosis of COVID-19. A zoom view of the design MS swab device and the steps for analysis. The insert shows two conduits for the incoming solvent (1) and aspiration of the solvent containing the extracted molecules (2) and a middle reservoir (3). During analysis, the swab is inserted into the middle reservoir. Upon the pressing of a foot pedal, the solvent is delivered to the middle reservoir to interact with the swab tip to extract molecules. After 10 s, the solvent containing the extracted molecules is transported to the mass spectrometer for ESI analysis.

their swab samples collected, 171 met the criteria of the time interval to PCR-sample collection and days from symptom onset. Demographic and clinical information for the patients from which the selected samples were obtained is provided in Tables 1 and S1. Based on the selection criteria, two statistical classifiers were generated: (1) asymptomatic COVID-19 PCR-negative (n = 101) vs COVID-19 symptomatic PCR-positive (n = 44) samples and (2) COVID-19 PCR-negative (n = 101 asymptomatic and n = 26 symptomatic) vs COVID-19 symptomatic PCR-positive. CV (10-fold) was used with Lasso to generate predictive models. For Classifier 1, the data were randomly split into a training set (2/3 of data, n = 97) and a validation set (1/3 of data, n = 48). Additionally, we tested Classifier 1 on a withheld test set of PCR-negative symptomatic samples (n = 26). The performance of the models was evaluated by measuring the predictive accuracy, sensitivity, specificity, negative predictive value (NPV), and positive predictive value (PPV), which were calculated based on the agreement with PCR diagnosis. Statistical analyses were performed by K.Y.G., M.F.K., J.Q.L., and J.M.G., and independently verified by R.T. The Supporting Information describes detailed data preprocessing, inclusion criteria for statistical analysis, and details on Lasso and other statistical methods.

RESULTS

Design of the MasSpec Pen-ESI System. We previously developed the MasSpec Pen as a handheld device directly coupled to a mass spectrometer for direct analysis of tissues.[37] The PDMS pen tip was composed of a solvent reservoir that held a solvent droplet in contact with a sample surface to enable efficient molecular extraction. While this design is intuitive for handheld use and well-suited for the analysis of tissue regions, the area covered by the reservoir opening (typically ~5.7 mm^2) was insufficient for uniform sampling and analysis of the secretion covering the three-dimensional area of an entire swab tip. To enable sensitive and robust analysis of all of the mucous secretion material in and on a swab tip, we thus redesigned and optimized the MasSpec Pen device, interface, and ionization system with the goal of ensuring direct and efficient sampling of the entire swab tip while maintaining the ease-of-use and rapid nature of the analysis of the original MasSpec Pen. The PDMS swab sampling device was integrated via PTFE tubing with a subatmospheric pressure ESI source for effective ionization and sensitive analysis of the extracted molecules (Figure 1). Similar to the original MasSpec Pen PDMS tip, the PDMS sampling unit is designed with three conduits that connect to a middle reservoir that was widened to 5.5 mm diameter and ~22 mm height to enable an entire swab tip to be fully inserted (Figure 1, insert). A PTFE tube connected to a syringe pump was then inserted into conduit 1 for the delivery of the solvent to the middle reservoir, whereas a second PTFE tube was inserted into conduit 2 for solvent aspiration into the subatmospheric pressure ESI source. The swab analysis is then performed with minimal operational steps: after the swab is inserted into the middle swab reservoir, solvent is delivered to the reservoir through a PTFE tube connected to conduit 1 via the pressing of a foot pedal, where the solvent interacts with the entire swab tip for 10 s for analyte extraction. Following the extraction period, conduit 2 is

https://doi.org/10.1021/acs.analchem.1c01937
Anal. Chem. XXXX, XXX, XXX−XXX

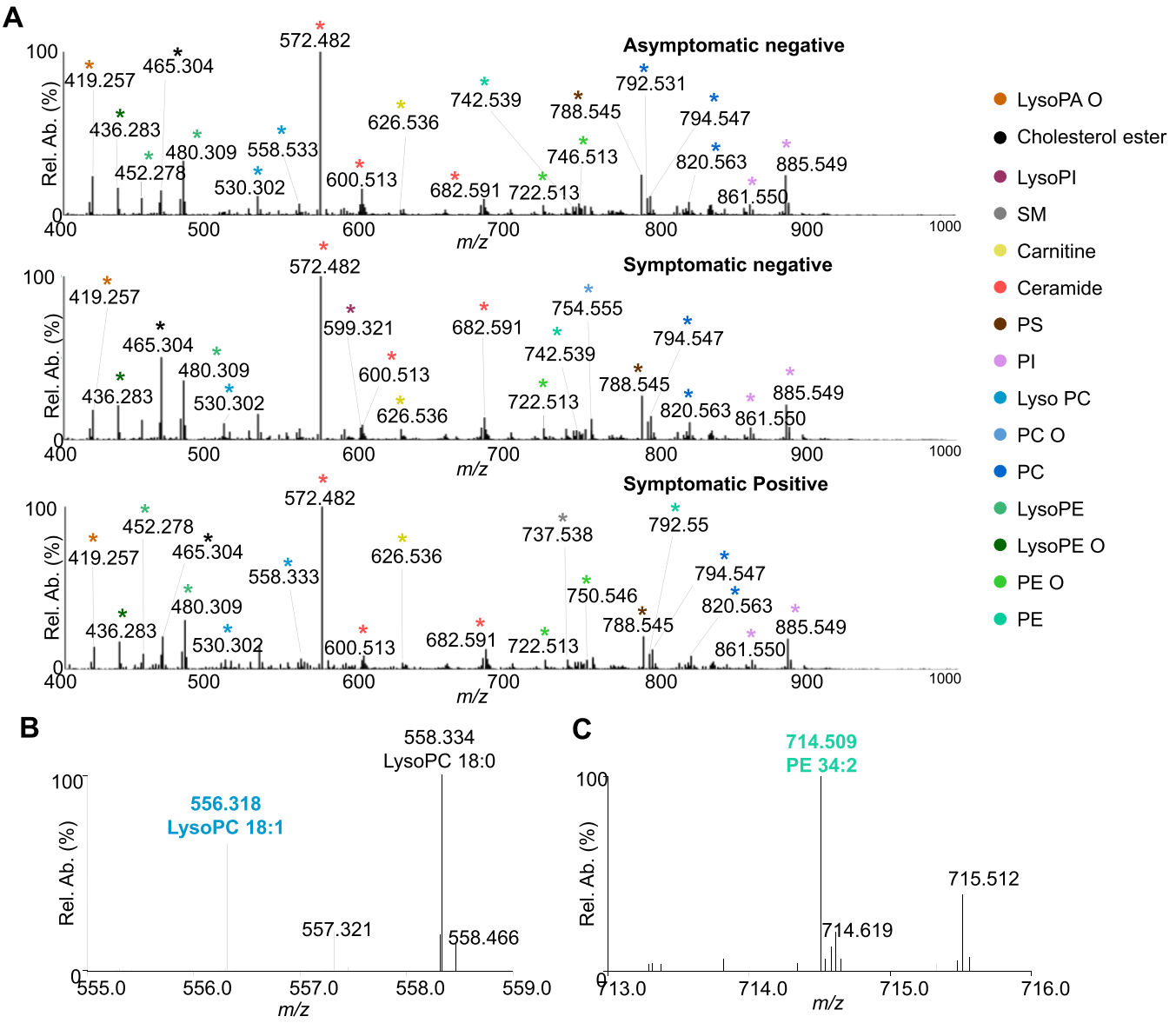

Figure 2. MasSpec Pen-ESI MS analysis of asymptomatic negative, symptomatic negative, and symptomatic positive samples in the negative ion mode. (A) Averaged spectra of all asymptomatic negative (n = 101, top), symptomatic negative (n = 26, middle), and symptomatic positive (n = 44, bottom). Different colored peaks correspond to different lipid classes, which are labeled in the legend. (B) Zoom in of the m/z range of 555−559 to show the detection of m/z 556.318 and m/z 558.334 ions tentatively identified lysoPC 18:1 and lysoPC 18:0, respectively. (C) Zoom in of the m/z range of 713−716 to show the detection of m/z 714.509 tentatively identified PE 34:2.

opened for 30 s allowing the vacuum to aspirate the solvent to the sprayer for ESI analysis. Within the ESI source, a lab-built sprayer promotes ionization of the molecules extracted within the solvent. Note that a subatmospheric pressure was set within the ESI housing, measured via the forevacuum pressure of the mass spectrometer (1.4−1.6 mbar), with the sole purpose of enabling suction and thus transport of the solvent from the swab reservoir to the ESI sprayer.

Optimization of the MasSpec Pen-ESI System for Swab Analysis. Using the MasSpec Pen-ESI system coupled to an LTQ-Orbitrap XL mass spectrometer, we first evaluated commonly used medical polyester and nylon flock swabs sterilized with ethylene oxide or γ irradiation for assay compatibility by dipping the swabs in a solution of CL 72:4 standard followed by analysis using MasSpec Pen-ESI MS. For the analysis of nylon flock swabs sterilized using ethylene oxide, a series of interfering ions identified as repeating units of ethylene oxide were observed from m/z 350−1200 at a ∼5.5-fold (n = 5, m/z 735.420) higher relative abundance compared to the CL standard ion of m/z 727.510 (Figure S1), thus hindering the detection of the CL standard due to ion suppression. Yet, no polymer ions were observed in the mass spectra obtained from polyester flock swabs sterilized with γ irradiation. Thus, all consecutive experiments including collection and analysis of clinical samples were therefore performed with polyester flock swabs sterilized by γ irradiation to avoid polymer interference.

Next, solvent composition and the volume used to fill the reservoir were optimized to ensure that the entire swab was saturated with the solvent to efficiently extract molecules, as well as allow for consistent signal and ESI spray stability during the analysis. Different organic solvent systems with volumes ranging from 100 to 200 μL were evaluated, with a solvent volume of 167 μL selected as optimal. Among the solvent

https://doi.org/10.1021/acs.analchem.1c01937
Anal. Chem. XXXX, XXX, XXX−XXX

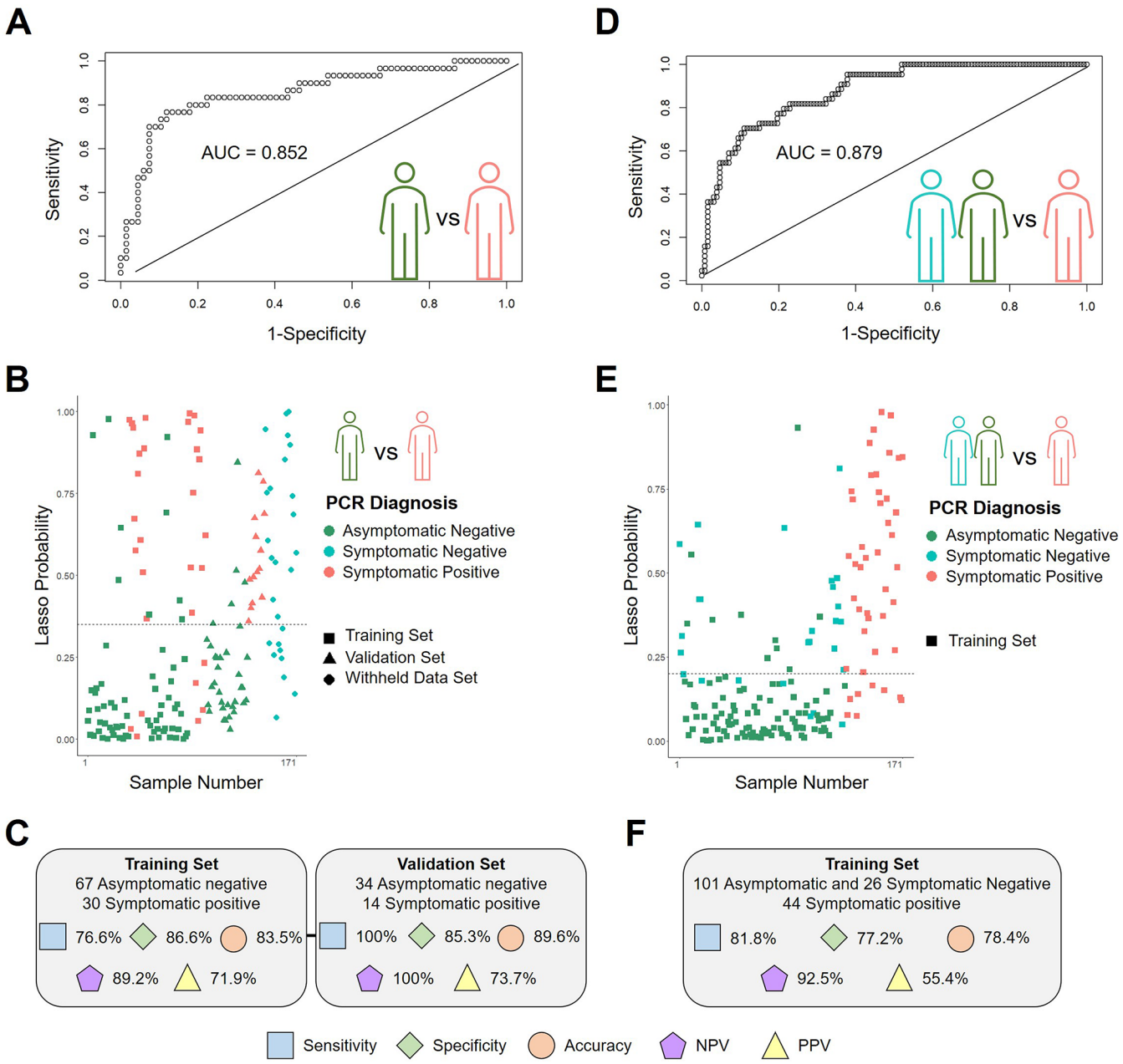

Figure 3. Statistical analysis results for classification models 1 and 2. Classifier 1, asymptomatic negative vs symptomatic positive, (A) ROC curve, and (B) plot of the classification probabilities for samples used in the training and validation set. The dashed line represents the cutoff value for classification as asymptomatic negative or symptomatic positive for COVID-19 (0.350). (C) Sensitivity, specificity, accuracy, NPV, and PPV for the training and validation set for Lasso Classifier 1. Classifier 2, negative vs positive, (D) ROC curve, and (E) plot of the classification probabilities for samples used in the training for Classifier 2. The dashed line represents the cutoff value for classification as negative or positive for COVID-19 (0.201). (F) Sensitivity, specificity, accuracy, NPV, and PPV for the training set for Lasso Classifier 2.

systems tested, $CHCl_3$/MeOH (1:1, v/v) yielded the highest reproducibility (relative standard deviation of 6.4% (n = 10)) and spray stability (~20−30 s of ion signal) while minimizing the extraction and detection of interfering ions. Notably, a 25.5% (n = 4) increase in the signal intensity of lipids was achieved when compared to the traditional MasSpec Pen setup[38] (Figure S2), likely due to more efficient ionization and desolvation provided by ESI. Altogether, a total analysis time of 45 s or less per swab was achieved, which included 5 s of solvent delivery, 10 s of swab extraction time, and ~20−30 s droplet transport and ESI signal (Figure 1). Lastly, we evaluated if heat inactivation led to any substantial change or degradation to the lipids contained in the sample using PG and PE lipid standards (Figure S3). We found no statistical significance (p > 0.05) in the mean intensity of the lipid standards detected from the heat-inactivated or control swabs, although other nonspecific unknown ions from polyester swab tip material were observed at qualitatively different relative abundances. These results indicate that the inactivation process did not significantly alter the lipid composition.

Molecular Analysis of Clinical Nasopharyngeal Swabs. To evaluate if lipid information diagnostic of COVID-19 disease could be extracted from viral transport media, lipid extracts were prepared from the media and

https://doi.org/10.1021/acs.analchem.1c01937
Anal. Chem. XXXX, XXX, XXX−XXX

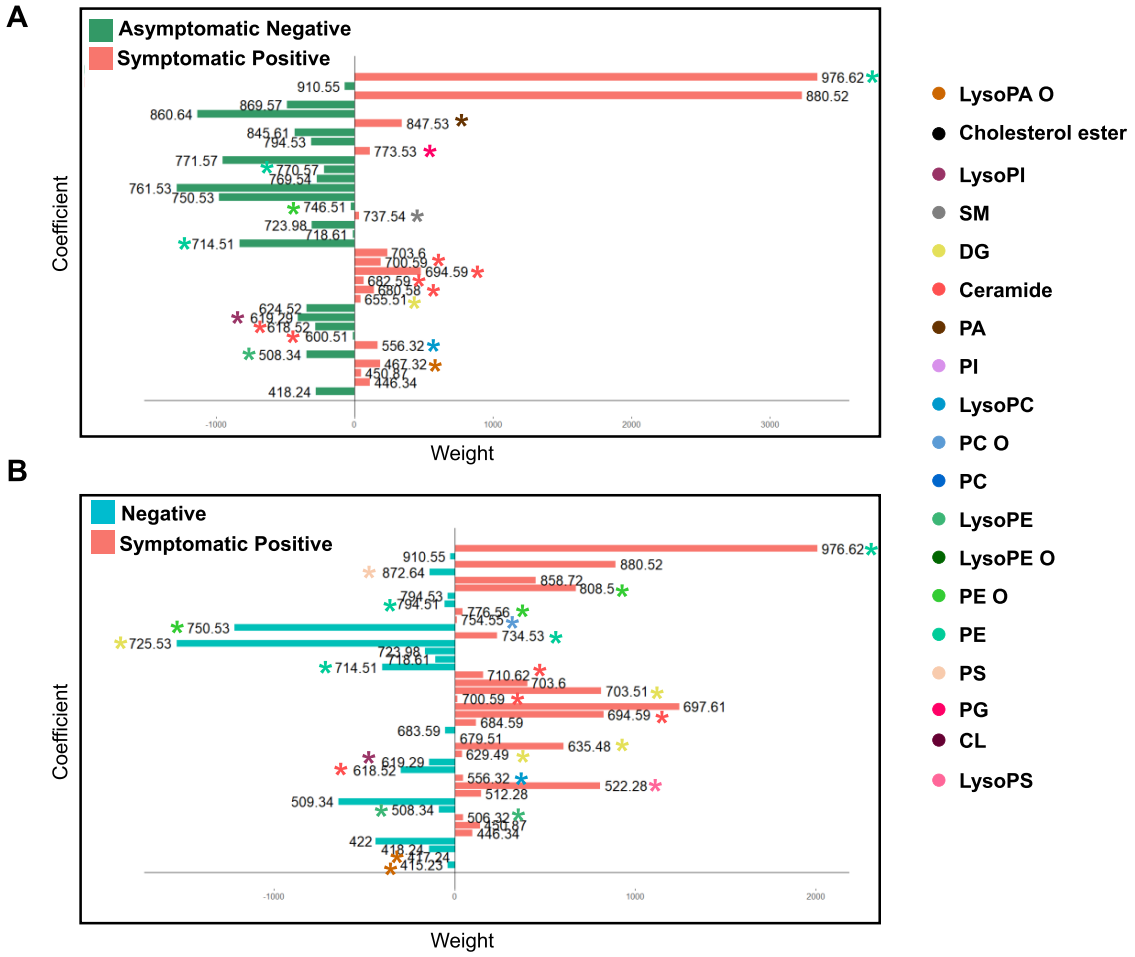

Figure 4. Lasso classification features. Features (m/z) selected as indicative of negative infection (negatively weighted values) and positive SARS-CoV-2 infection (positively weighted values) for (A) Classifier 1 and (B) Classifier 2. Tentatively identified features are color-coded with asterisks corresponding to the identified lipid class.

analyzed using ESI in the negative ion mode. The mass spectra presented high relative abundances of interfering polymer molecules, with few lipid species detected at low relative abundances (Figure S1). As such, we assessed the ability of the MasSpec Pen to extract lipid species directly from the clinical nasal swabs that were stored in a dry transport tube (with no media). As Figure 2A shows, we observed rich molecular profiles in the negative ion mode composed of a diverse range of glycerophospholipid and lysolipid species in mass spectral profiles of symptomatic COVID-19 positive and negative swabs and asymptomatic healthy samples. Deprotonated ($[M - H]^-$) and chlorinated ($[M + Cl]^-$) lipid species were observed in the mass spectra for all samples analyzed. Note that the m/z 400−1000 range was used to avoid detection and ion suppression from nonbiological interferents detected as ions of m/z < 400 while enabling detection of a broad range of lipid species. Various ions such as lysoPE 16:0 (m/z 452.278), lysoPE 18:0 (m/z 480.309), lysoPC 18:1 (m/z 556.318) (Figure 2B), and cholesterol sulfate (m/z 465.304) were observed in the m/z range 400−600 and identified via tandem MS and high mass accuracy measurements (<5 ppm). Additionally, molecules such as ceramide species including Cer 34:1 (m/z 572.481), Cer 36:1 (m/z 601.533), and Cer 42:2 (m/z 682.591) as well as glycerophospholipids including PS 18:1_18:0 (m/z 788.545), PI 20:4_18:0 (m/z 885.550), and PE 34:2 (m/z 714.509) were observed (Figure 2C).

Statistical Prediction of COVID-19 Infection. We next statistically evaluated if the molecular information obtained with the MasSpec Pen-ESI MS system was predictive of COVID-19 infection. We first employed the Lasso method to build a classification model to discriminate data obtained from symptomatic patients positive for COVID-19 (n = 44) and asymptomatic individuals negative for COVID-19 (n = 101), termed Classifier 1. The model exhibited a strong performance using 10-fold CV (n = 97), yielding an area under the receiver operating characteristic (ROC) curve (AUC) of 0.852 (Figure 3A) and an accuracy of 83.5% (Figure 3C). A prediction probability value of 0.350 was selected as the optimal threshold value for sample classification based on the ROC curve. Samples with a probability lower than 0.350 were classified as asymptomatic negative and those with a probability higher than 0.350 were classified as symptomatic positive (Figure 3B). Using this approach, a total of 58 out of 67 asymptomatic negative and 23 out of 30 symptomatic positive samples had a prediction result in agreement with PCR, resulting in 76.7% sensitivity and 86.6% specificity (Figure 3C). We also calculated the NPV and PPV to evaluate the ability of our statistical classifier to provide a predictive COVID-19 diagnosis that aligns with the true absence or presence of the disease. The model yielded an NPV of 89.2% and a PPV of 71.9%.

Next, we assessed the predictive performance of Classifier 1 using a validation set of 34 asymptomatic negative and 14

https://doi.org/10.1021/acs.analchem.1c01937
Anal. Chem. XXXX, XXX, XXX−XXX

symptomatic positive samples. Only five asymptomatic negative samples were classified as positive in disagreement with PCR, while all symptomatic positive samples were correctly classified, resulting in an overall agreement with PCR of 89.6%, a specificity of 85.3%, a sensitivity of 100%, NPV of 100%, and PPV of 73.7%. We then used the classifier to predict on a withheld set of samples obtained from patients presenting respiratory symptoms similar to those associated with the COVID-19 disease (n = 26) but had a negative PCR result (Table S1). A total of 9 samples in the withheld set of data were classified as negative in agreement with PCR, whereas 17 samples were classified as positive, in disagreement with the PCR diagnosis. Out of these 17 patients, 12 had a chest computational tomography (CT) that was suggestive of viral infection, presenting ground-glass opacity (GGO) among other features such as consolidation and pulmonary commitment.[39] Table S2 provides a detailed summary of the classification results.

To more broadly evaluate the performance for COVID-19 screening, we built a second classifier, termed Classifier 2, that combined the samples from the symptomatic negative patients (n = 26) and the asymptomatic negative individuals (n = 101) into a single negative class, whereas the positive class was comprised by samples from symptomatic positive patients (n = 44). The predictive model was comprised of 41 m/z features and yielded an overall agreement with PCR of 78.4%, sensitivity of 81.8%, specificity of 77.2% (Figure 3F), and an AUC of 0.879 (Figure 3D). A prediction probability threshold of 0.201 was selected to maximize the sensitivity of Classifier 2 (Figure 3E). A total of 29 PCR negative samples were classified as positive by our method, 19 among which were from symptomatic patients that presented respiratory symptoms similar to those associated with the COVID-19 disease. We also noted that 13 of the 19 symptomatic negative samples classified as positive had chest CT results suggestive of viral infection.

Among the selected features used to build the two classification models, various lipids were selected to discriminate the COVID-19 positive disease and negative diagnosis. For example, several PE and lysoPE species were selected as important for predicting negative status among the two classifiers generated, including lysoPE 20:0 (m/z 508.341) and PE 34:2 (m/z 714.508), (Figure 4). For Classifier 1, various ceramides such as Cer 42:3 (m/z 680.576), Cer 42:2 (m/z 682.591), Cer 43:3 (m/z 694.592), and Cer 44:5 (m/z 700.587) were selected as characteristic of symptomatic positive COVID-19 infection by Lasso, whereas PE 38:2 (m/z 770.571) and lysoPI 20:4 (m/z 619.289) were selected as indicative of asymptomatic negative samples (Figure 4A). Other species such as PE 50:9 (m/z 976.619) and lysoPC 18:1 (m/z 556.317) were selected as important for classification and weighted toward symptomatic positive COVID-19 disease for Classifier 1 and 2 (Figure 4A,B). LysoPS 18:1 (m/z 522.284) and DG 40:6 (m/z 808.504) were selected by Lasso as predictive of COVID-19 positive infection for Classifier 2 (Figure 4B). Table S3 provides the Lasso features selected for all statistical classifiers, the corresponding identifications, and mass errors.

The results from the descriptive statistical analysis performed to compare the clinical characteristics among the two symptomatic groups, symptomatic COVID-19 PCR positive and COVID-19 PCR negative subjects, are shown in Table 1. No association was found among the occurrence of symptoms and comorbidities with the PCR result. These results indicate that there is no clinical difference detected by the symptomatic PCR-positive and symptomatic PCR-negative groups within the patients in our study.

DISCUSSION

With the slow rollout of the COVID-19 vaccines, a recurring global surge in cases, and the discovery of variants with increased rates of transmission, the availability of alternative technologies that offer rapid analysis and screening for COVID-19 is highly desirable to meet unceasing testing demands. We describe, herein, the development of a robust MasSpec Pen-ESI MS system for rapid swab analysis and applied the technology to the analysis of nasopharyngeal swabs to evaluate its usefulness for COVID-19 screening.

Modifications were made to the MasSpec Pen design and system to improve the performance and sensitivity for the analysis of swabs. Larger sampling area capabilities were attained to ensure that three-dimensional clinical swabs with a sparse and heterogeneous distribution of biological material were sampled in their entirety. The modified PDMS tip includes a hollow middle channel designed to fit a single swab tip and allows full coverage and extraction of molecular information from the entire sample during analysis. The modified PDMS tip includes a hollow middle channel to fit a single swab tip that allowed the full covering and extraction of molecular information from the entire sample during analysis (Figure 1). Thus, the MasSpec Pen-ESI MS system enables direct, rapid, efficient, and uniform sampling of all of mucous secretion on the swab and largely mitigating bias in the data due to uneven sampling. Additionally, the use of ESI increased the ionization efficiency of extracted lipid molecules and improved the sensitivity for the untargeted molecular analysis of swabs, enabling the detection of abundant ions and molecular profiles from the biological sample. Further, the MasSpec Pen-ESI system using $CHCl_3$/MeOH as a solvent allowed detection of predominantly deprotonated lipid species compared to the traditional MasSpec Pen setup using water as the solvent, which resulted in the detection of deprotonated lipids as well as sodium adducts (Figure S2). While we speculate the different solvent systems may have played a role in the changes observed in the mass spectra, more studies are needed to systematically evaluate these trends. Of note, while the total time per analysis of 45 s is remarkably fast compared to other available molecular tests, additional system automation approaches are being explored to further expedite device swapping between samples and thus maximize testing throughput. Importantly, similar to the original handheld system, this design of the device maintains a small footprint, retains the ease-of-use, plug-and-play and disposability features, is capable of performing rapid molecular analysis, and is compatible with multiple mass spectrometers fitted with ESI interfaces, potentially facilitating implementation in clinical laboratories already equipped with MS instrumentation.

We applied the MasSpec Pen-ESI MS system to analyze 244 nasopharyngeal swabs from COVID-19 positive and negative patients, from which 171 were used to build two statistical classifiers based on the lipid profiles obtained. Classifier 1 was built to evaluate the performance of our method in discriminating patients diagnosed as positive for COVID-19 infection by PCR from completely asymptomatic patients with a PCR negative result. The classifier was built using 145 samples and yielded a CV prediction accuracy of 83.5%, similar

https://doi.org/10.1021/acs.analchem.1c01937
Anal. Chem. XXXX, XXX, XXX−XXX

to what was achieved in a study using metabolite and lipid information obtained from DESI-MS (86%, n = 70) and LD-REIMS (84%, n = 70) analysis of heat-inactivated swabs from negative patients with previous SARS-CoV-2 infection and symptomatic positive patients.[32] We evaluated Classifier 1 on a validation set of 34 asymptomatic PCR-negative and 14 symptomatic PCR-positive samples, yielding a specificity of 85.3% or a low FPR of 14.7%, and most notably, a sensitivity of 100% or low FNR of 0%. These results demonstrate the ability of the MasSpec Pen-ESI technology to detect alterations in the lipid profiles of symptomatic patients with an active SARS-CoV-2 viral infection compared to healthy individuals and to build classification models based on detected lipid species.

We then used Classifier 1 to predict on a withheld set samples obtained from 26 symptomatic patients hospitalized with moderate or severe symptoms including fever, cough, difficulty in breathing, but received a negative PCR result for COVID-19 (Table S1). Nine of the symptomatic negative samples had a prediction result in agreement with PCR, while 17 symptomatic negative samples were classified as positive, in disagreement with PCR. Interestingly, 12 of the 17 symptomatic negative samples predicted as positive were obtained from patients showing GGO and consolidations in their chest CT scans, and five of the seven samples predicted as negative presented chest CT results indicative of being negative of viral infection. For example, sample 34 was obtained from a 76-year-old male patient who received a PCR negative diagnosis and was classified as positive by our method. This patient was experiencing cough, sore throat, and dyspnea, and had chest CT features suggestive of infection such as GGO, consolidations, and 50% pulmonary commitment. The patient was hospitalized in the intensive care unit for 13 days with the assistance of a mechanical ventilator until succumbing to death. Additional cases with similar clinical symptoms and results are described in the Supporting Information. Note that chest CT has been suggested as a fundamental tool for early diagnosis and monitoring of COVID-19 as it enables detection of lung alterations in symptomatic patients that are suggestive of viral infection.[40−43] In a recent study, a 90% sensitivity was reported for COVID-19 diagnosis based on GGO combined with other CT features.[44] Yet, chest CT is less specific than PCR and unable to distinguish between an active or previous SARS-CoV-2 infection or a different viral infection causing severe respiratory symptoms. It is also important to note that although PCR is the gold standard for COVID-19 detection and is highly accurate, several studies have reported a sensitivity of 80−90% (or FNR of 10−20%) for COVID-19 diagnosis using nasopharyngeal swabs.[45−47] Thus, while the results obtained on the withheld set of symptomatic PCR negative samples indicate the selected predictive lipid species comprising Classifier 1 are more strongly associated with the infection status, it is also possible that a proportion of the symptomatic PCR negative samples obtained from hospitalized patients may have inaccurate PCR results.

To more broadly evaluate the ability of our method to identify individuals negative for COVID-19 disease including symptomatic patients, we built Classifier 2 using a training set of symptomatic positive samples (n = 44) and a negative class (n = 127) composed of data from both symptomatic and asymptomatic PCR negative samples. As a limited number of symptomatic negative samples were used in Classifier 2, only a training set of samples was used to assess the performance of the model for COVID-19 screening. Using CV, Classifier 2 yielded a 78.4% overall agreement with PCR results, 81.8% sensitivity (FNR of 18.2%), and 77.2% specificity (FPR of 22.8%), similar to what was achieved for the training set of Classifier 1 despite the incorporation of symptomatic negative samples into the negative class. Of the 65 samples classified as positive by our method, 36 were from symptomatic positive samples, yielding a PPV value of 55.4%, meaning that for the prevalence of the disease in the cohort of patients evaluated (25.7%), 55.4% of patients with a positive prediction result by our method were also diagnosed as positive for COVID-19 by PCR. However, for the same disease prevalence, a high NPV of 92.5% was achieved, meaning that 92.5% of patients with a negative prediction by our method also received a negative PCR result for COVID-19. Thus, the high NPV value of 92.5% and the FNR of 18.2% achieved provide evidence that Classifier 2 can potentially identify individuals negative for SARS-CoV-2 infection and predict patients with SARS-CoV-2 infection as positive for the disease, both of which are paramount to halting the spread of the COVID-19 disease. While these results are encouraging, a larger cohort of samples is needed to validate the results by Classifiers 1 and 2 and further refine and improve the performance and robustness of the model for distinguishing symptomatic COVID-19 positive disease from symptomatic patients with other viral respiratory infections, such as the common cold and influenza.

Our statistical models were based on various classes of phospholipid species previously reported to play key roles in coronavirus virion production and replication[21,22,34] and that are major components of host cellular membranes. The tentatively identified lipids included glycerophospholipids, such as ceramides, lysolipids, and PE. Among those, several lysoPC species including lysoPC 18:1 were selected as predictive of the symptomatic COVID-19 positive disease. Interestingly, in a study by Yan et al., lysoPC species were detected at higher abundances in cells infected with the human coronavirus HCoV-229E, when compared to healthy cells, which substantiates our findings.[22] Yet, a recent study by Delafiori et al. reported decreased abundances of lysoPC species in the serum of COVID-19 positive patients.[33] Across both classifiers, PE 50:9 was selected as indicative of COVID-19 with the highest weight toward the disease, while other PE species such as PE 34:2 was selected as indicative of being negative for COVID-19. Increased abundance of PE species was also recently reported by Ford et al. in nasal swabs from COVID-19 positive patients.[32] Importantly, since our method does not enable deconvolution between the lipid signal arising from the virion or from host cells, we speculate that the species observed as indicative of COVID-19 are a major component of the virion cellular membrane and/or have increased abundances in host infected cells to enable replication of the virus. Thus, although lipid species represent promising detection targets for COVID-19, additional research is needed to elucidate the role of these species in the COVID-19 disease and host response to the infection.

This study has a few limitations. Concerning clinical samples, the swabs for MS and PCR analysis were collected separately for hospitalized patients in our study, which could potentially lead to discrepancies in their diagnoses, especially considering the reported FNR of PCR analysis.[45−47] Viral load information was also unavailable for the patients, which prevented evaluation of a potential relationship between viral burden, molecular information, and diagnostic performance achieved. Heat-inactivation was also used in our study for all of

https://doi.org/10.1021/acs.analchem.1c01937
Anal. Chem. XXXX, XXX, XXX−XXX

the clinical swabs, and thus, biosafety considerations in swab collection, storage, and inactivation steps are needed in future studies to facilitate sample collection and transport. Lastly, although our study was performed using a restricted population of individuals from Brazil, the promising results obtained warrant further investigation, and we expect that a larger cohort of patient samples including asymptomatic PCR positive patients and patients with other viral infections causing similar symptoms to COVID-19 will allow further refinement and validation of the classifiers for COVID-19 disease prediction using lipid information.

In conclusion, the integration of a redesigned version of the disposable MasSpec Pen device provides a rapid MS-based screening method for COVID-19 disease directly from nasopharyngeal swabs. Modifications to the sampling unit and coupling to ESI enabled more effective and reproducible extraction and ionization of lipids from COVID-19 clinical nasal swabs using common solvent systems while maintaining the disposability and user-friendly features of the MasSpec Pen device. As the MasSpec Pen-ESI system has a small footprint and is compatible with various mass spectrometers, this system could be potentially implemented in clinical laboratories and testing facilities that are currently suited with MS instrumentation. The speed of analysis (~45 s/swab) combined with a relatively lower FNR compared to other FDA-approved screening methods and high NPV value achieved substantiate the potential of the technology as a rapid screening tool to identify individuals negative for COVID-19 infection prior to or when PCR is not readily available. While further refinement and testing of the methodology and statistical classifiers with larger sample cohorts will be pursued to improve analytical and diagnostic performance, the present results point to the MasSpec Pen-ESI MS system as a valuable approach for rapid screening of clinical swabs on a seconds-to-minutes time scale.

■ ASSOCIATED CONTENT

Supporting Information

The Supporting Information is available free of charge at https://pubs.acs.org/doi/10.1021/acs.analchem.1c01937.

Additional experimental details and methods, including tables containing clinical information for symptomatic negative patients, m/z values or features included in the Lasso classification models, a summary of Lasso classification results, figures showing a mass spectrum from the MasSpec Pen-ESI analysis of nylon flock swabs, mass spectra obtained from the MasSpec Pen with ESI or solvent-assisted inlet ionization, a comparison of mass spectra from the analysis of swabs with and without heat inactivation, and a mass spectrum from ESI analysis of viral transport media (PDF)

■ AUTHOR INFORMATION

Corresponding Authors

Livia S. Eberlin − *Department of Chemistry, The University of Texas at Austin, Austin, Texas 78712, United States;* orcid.org/0000-0002-3885-3215; Email: liviase@utexas.edu

Andreia M. Porcari − *MS4Life Laboratory of Mass Spectrometry, Health Sciences Postgraduate Program, São Francisco University, Bragança Paulista, São Paulo 12916-900, Brazil;* orcid.org/0000-0003-4244-8594; Email: andreia.porcari@usf.edu.br

Authors

Kyana Y. Garza − *Department of Chemistry, The University of Texas at Austin, Austin, Texas 78712, United States*

Alex Ap. Rosini Silva − *MS4Life Laboratory of Mass Spectrometry, Health Sciences Postgraduate Program, São Francisco University, Bragança Paulista, São Paulo 12916-900, Brazil*

Jonas R. Rosa − *MS4Life Laboratory of Mass Spectrometry, Health Sciences Postgraduate Program, São Francisco University, Bragança Paulista, São Paulo 12916-900, Brazil*

Michael F. Keating − *Department of Chemistry, The University of Texas at Austin, Austin, Texas 78712, United States*

Sydney C. Povilaitis − *Department of Chemistry, The University of Texas at Austin, Austin, Texas 78712, United States*

Meredith Spradlin − *Department of Chemistry, The University of Texas at Austin, Austin, Texas 78712, United States*

Pedro H. Godoy Sanches − *MS4Life Laboratory of Mass Spectrometry, Health Sciences Postgraduate Program, São Francisco University, Bragança Paulista, São Paulo 12916-900, Brazil*

Alexandre Varão Moura − *MS4Life Laboratory of Mass Spectrometry, Health Sciences Postgraduate Program, São Francisco University, Bragança Paulista, São Paulo 12916-900, Brazil*

Junier Marrero Gutierrez − *MS4Life Laboratory of Mass Spectrometry, Health Sciences Postgraduate Program, São Francisco University, Bragança Paulista, São Paulo 12916-900, Brazil*

John Q. Lin − *Department of Chemistry, The University of Texas at Austin, Austin, Texas 78712, United States;* orcid.org/0000-0001-5888-3107

Jialing Zhang − *Department of Chemistry, The University of Texas at Austin, Austin, Texas 78712, United States*

Rachel J. DeHoog − *Department of Chemistry, The University of Texas at Austin, Austin, Texas 78712, United States*

Alena Bensussan − *Department of Chemistry, The University of Texas at Austin, Austin, Texas 78712, United States*

Sunil Badal − *Department of Chemistry, The University of Texas at Austin, Austin, Texas 78712, United States*

Danilo Cardoso de Oliveira − *MS4Life Laboratory of Mass Spectrometry, Health Sciences Postgraduate Program, São Francisco University, Bragança Paulista, São Paulo 12916-900, Brazil*

Pedro Henrique Dias Garcia − *MS4Life Laboratory of Mass Spectrometry, Health Sciences Postgraduate Program, São Francisco University, Bragança Paulista, São Paulo 12916-900, Brazil*

Lisamara Dias de Oliveira Negrini − *Municipal Department of Health, Bragança Paulista, Sao Paulo 12902-230, Brazil;* Present Address: Universidade São Francisco, Bragança Paulista, SP, Brazil

Marcia Ap. Antonio − *Integrated Unit of Pharmacology and Gastroenterology, UNIFAG, Bragança Paulista, Sao Paulo 12916-900, Brazil*

Thiago C. Canevari − *School of Material Engineering and Nanotechnology, MackMass Laboratory, Mackenzie Presbyterian University, São Paulo, SP 01302-907, Brazil*

https://doi.org/10.1021/acs.analchem.1c01937
Anal. Chem. XXXX, XXX, XXX−XXX

Marcos N. Eberlin − *School of Material Engineering and Nanotechnology, MackMass Laboratory, Mackenzie Presbyterian University, São Paulo, SP 01302-907, Brazil*
Robert Tibshirani − *Department of Biomedical Data Science, Stanford University, Stanford, California 94305, United States*

Complete contact information is available at: https://pubs.acs.org/10.1021/acs.analchem.1c01937

Author Contributions

[▽]K.Y.G. and A.A.R.S. contributed equally to this work.

Author Contributions

L.S.E., M.N.E., and A.M.P. conceived and designed the research; K.Y.G., M.F.K., J.Z., and L.S.E. designed the MasSpec Pen system; K.Y.G., M.F.K., S.C.P., M.S., J.Z., R.J.D., A.B., and S.B., performed mass spectrometry experiments; A.R.S., J.R.R., P.H.G.S., A.V.M., D.C., and P.H.D.G. collected clinical swabs and clinical data; J.Q.L., J.M.G., K.Y.G, M.F.K., and R.T. performed statistical analysis; L.D.O.N. and M.A.A. performed and supervised clinical research; L.S.E., M.N.E., T.C.C., and A.M.P. provided funding and supervision for the study; K.Y.G., A.M.P., and L.S.E. wrote the manuscript; and all authors revised, read, and approved the final manuscript.

Notes

The authors declare the following competing financial interest(s): K.Y.G., M.F.K., S.C.P., J.Q.L., J.Z., and L.S.E. are inventors in US Patent No. 10,643,832 owned by Board of Regents of the University of Texas System and/or in a provisional patent application related to the MasSpec Pen Technology licensed to MS Pen Technologies, Inc. J.Z. and L.S.E. are shareholders in MS Pen Technologies, Inc. L.S.E. serves as chief scientific officer for MS Pen Technologies, Inc. All other authors declare no competing interests.
The data used in this study have been reported in Dataverse, https://doi.org/10.7910/DVN/6URYEH

■ ACKNOWLEDGMENTS

The authors are grateful to Genio Technologies, Inc., the Coordination for the Improvement of Higher Education Personnel (CAPES #88887.504805/2020-00), the São Paulo Research Foundation (grant 2019/04314-6), MackPesquisa (grant 191003), and the Welch Foundation (award number F-1895-20190330 to LSE) for funding this study. The authors also thank UNIFAG, Santa Casa, Bragantino Hospitals, and their clinical staff for facilitating and contributing to sample collection, as well as the authors also acknowledge Dr. Scott Hunicke-Smit from the Clinical Pathology Laboratories (Austin, TX) for providing samples for research. The authors are very thankful to every volunteer who accepted to participate in this study. They are also grateful to Tim Hooper for his assistance with the lab-built ESI source.

■ REFERENCES

(1) Huang, C.; Wang, Y.; Li, X.; Ren, L.; Zhao, J.; Hu, Y.; Zhang, L.; Fan, G.; Xu, J.; Gu, X.; Cheng, Z.; Yu, T.; Xia, J.; Wei, Y.; Wu, W.; Xie, X.; Yin, W.; Li, H.; Liu, M.; Xiao, Y.; et al. *Lancet* **2020**, *395*, 497−506.
(2) Wu, F.; Zhao, S.; Yu, B.; Chen, Y. M.; Wang, W.; Song, Z. G.; Hu, Y.; Tao, Z. W.; Tian, J. H.; Pei, Y. Y.; Yuan, M. L.; Zhang, Y. L.; Dai, F. H.; Liu, Y.; Wang, Q. M.; Zheng, J. J.; Xu, L.; Holmes, E. C.; Zhang, Y. Z. *Nature* **2020**, *579*, 265−269.
(3) Mina, M. J.; Parker, R.; Larremore, D. B. *N. Engl. J. Med.* **2020**, *383*, No. e120.
(4) Vandenberg, O.; Martiny, D.; Rochas, O.; van Belkum, A.; Kozlakidis, Z. *Nat. Rev. Microbiol.* **2020**, *19*, 171−183.
(5) Masterson, T. A.; Dill, A. L.; Eberlin, L. S.; Mattarozzi, M.; Cheng, L.; Beck, S. D.; Bianchi, F.; Cooks, R. G. *J. Am. Soc. Mass Spectrom.* **2011**, *22*, 1326−1333.
(6) Tromberg, B. J.; Schwetz, T. A.; Perez-Stable, E. J.; Hodes, R. J.; Woychik, R. P.; Bright, R. A.; Fleurence, R. L.; Collins, F. S. *N. Engl. J. Med.* **2020**, *383*, 1071−1077.
(7) Lisboa Bastos, M.; Tavaziva, G.; Abidi, S. K.; Campbell, J. R.; Haraoui, L. P.; Johnston, J. C.; Lan, Z.; Law, S.; MacLean, E.; Trajman, A.; Menzies, D.; Benedetti, A.; Ahmad Khan, F. *BMJ* **2020**, *370*, No. m2516.
(8) Miller, T. E.; Garcia Beltran, W. F.; Bard, A. Z.; Gogakos, T.; Anahtar, M. N.; Astudillo, M. G.; Yang, D.; Thierauf, J.; Fisch, A. S.; Mahowald, G. K.; Fitzpatrick, M. J.; Nardi, V.; Feldman, J.; Hauser, B. M.; Caradonna, T. M.; Marble, H. D.; Ritterhouse, L. L.; Turbett, S. E.; Batten, J.; Georgantas, N. Z.; et al. *FASEB J.* **2020**, *34*, 13877−13884.
(9) Abbasi, J. *JAMA* **2020**, *324*, No. 1386.
(10) Mak, G. C. K.; Lau, S. S. Y.; Wong, K. K. Y.; Chow, N. L. S.; Lau, C. S.; Lam, E. T. K.; Chan, R. C. W.; Tsang, D. N. C. *J. Clin. Virol.* **2021**, *134*, No. 104712.
(11) Prince-Guerra, J. L.; Almendares, O.; Nolen, L. D.; Gunn, J. K. L.; Dale, A. P.; Buono, S. A.; Deutsch-Feldman, M.; Suppiah, S.; Hao, L.; Zeng, Y.; Stevens, V. A.; Knipe, K.; Pompey, J.; Atherstone, C.; Bui, D. P.; Powell, T.; Tamin, A.; Harcourt, J. L.; Shewmaker, P. L.; Medrzycki, M.; et al. *Morb. Mortal. Wkly. Rep.* **2021**, *70*, 100−105.
(12) West, C. P.; Montori, V. M.; Sampathkumar, P. *Mayo Clin. Proc.* **2020**, *95*, 1127−1129.
(13) Abu-Farha, M.; Thanaraj, T. A.; Qaddoumi, M. G.; Hashem, A.; Abubaker, J.; Al-Mulla, F. *Int. J. Mol. Sci.* **2020**, *21*, No. 3544.
(14) Caterino, M.; Gelzo, M.; Sol, S.; Fedele, R.; Annunziata, A.; Calabrese, C.; Fiorentino, G.; D'Abbraccio, M.; Dell'Isola, C.; Fusco, F. M.; Parrella, R.; Fabbrocini, G.; Gentile, I.; Andolfo, I.; Capasso, M.; Costanzo, M.; Daniele, A.; Marchese, E.; Polito, R.; Russo, R.; et al. *Sci. Rep.* **2021**, *11*, No. 2941.
(15) Ivanova, P. T.; Myers, D. S.; Milne, S. B.; McClaren, J. L.; Thomas, P. G.; Brown, H. A. *ACS Infect. Dis.* **2015**, *1*, 435−442.
(16) Nayak, D. P.; Hui, E. K. W. *Membrane Dynamics and Domains: Subcellular Biochemistry*; Quinn, P. J., Ed.; Springer US: Boston, MA, 2004; pp 443−491.
(17) Quigley, J. P.; Rifkin, D. B.; Reich, E. *Virology* **1971**, *46*, 106−116.
(18) Kates, M.; Allison, A. C.; Tyrrell, D. A. J.; James, A. T. *Biochim. Biophys. Acta* **1961**, *52*, 455−466.
(19) Callens, N.; Brügger, B.; Bonnafous, P.; Drobecq, H.; Gerl, M. J.; Krey, T.; Roman-Sosa, G.; Rümenapf, T.; Lambert, O.; Dubuisson, J.; Rouillé, Y. *PLoS Pathog.* **2016**, *12*, No. e1005476.
(20) Dou, D.; Revol, R.; Ostbye, H.; Wang, H.; Daniels, R. *Front. Immunol.* **2018**, *9*, No. 1581.
(21) Van Genderen, I. L.; Godeke, G. J.; Rottier, P. J. M.; Van Meer, G. *Biochem. Soc. Trans.* **1995**, *23*, 523−526.
(22) Yan, B. P.; Chu, H.; Yang, D.; Sze, K. H.; Lai, P. M.; Yuan, S. F.; Shuai, H. P.; Wang, Y. X.; Kao, R. Y. T.; Chan, J. F. W.; Yuen, K. Y. *Viruses* **2019**, *11*, No. 73.
(23) Zhang, J.; Sans, M.; Garza, K. Y.; Eberlin, L. S. *Mass Spectrom. Rev.* **2020**, *40*, 692−720.
(24) Pu, F.; Chiang, S.; Zhang, W.; Ouyang, Z. *Analyst* **2019**, *144*, 1034−1051.
(25) Ho, Y. P.; Reddy, P. M. *Clin. Chem.* **2010**, *56*, 525−536.
(26) Ganova-Raeva, L. M.; Khudyakov, Y. E. *Expert Rev. Mol. Diagn.* **2013**, *13*, 377−388.
(27) Mahmud, I.; Garrett, T. J. *J. Am. Soc. Mass Spectrom.* **2020**, *31*, 2013−2024.
(28) Nachtigall, F. M.; Pereira, A.; Trofymchuk, O. S.; Santos, L. S. *Nat. Biotechnol.* **2020**, *38*, 1168−1173.
(29) Rocca, M. F.; Zintgraff, J. C.; Dattero, M. E.; Santos, L. S.; Ledesma, M.; Vay, C.; Prieto, M.; Benedetti, E.; Avaro, M.; Russo, M.;

Nachtigall, F. M.; Baumeister, E. *J. Virol. Methods* **2020**, *286*, No. 113991.
(30) De Silva, I. W.; Nayek, S.; Singh, V.; Reddy, J.; Granger, J. K.; Verbeck, G. F. *Analyst* **2020**, *145*, 5725−5732.
(31) Shen, B.; Yi, X.; Sun, Y.; Bi, X.; Du, J.; Zhang, C.; Quan, S.; Zhang, F.; Sun, R.; Qian, L.; Ge, W.; Liu, W.; Liang, S.; Chen, H.; Zhang, Y.; Li, J.; Xu, J.; He, Z.; Chen, B.; Wang, J.; et al. *Cell* **2020**, *182*, 59−72.e15.
(32) Ford, L.; Simon, D.; Balog, J.; Jiwa, N.; Higginson, J.; Jones, E.; Mason, S.; Wu, V.; Manoli, E.; Stavrakaki, S. M.; McKenzie, J.; McGill, D.; Koguna, H.; Kinross, J.; Takats, Z. *medRxiv* **2020**, No. 207647.
(33) Delafiori, J.; Navarro, L. C.; Siciliano, R. F.; de Melo, G. C.; Busanello, E. N. B.; Nicolau, J. C.; Sales, G. M.; de Oliveira, A. N.; Val, F. F. A.; de Oliveira, D. N.; Eguti, A.; Dos Santos, L. A.; Dalcoquio, T. F.; Bertolin, A. J.; Abreu-Netto, R. L.; Salsoso, R.; Baia-da-Silva, D.; Marcondes-Braga, F. G.; Sampaio, V. S.; Judice, C. C.; et al. *Anal. Chem.* **2021**, *93*, 2471−2479.
(34) Wu, D.; Shu, T.; Yang, X.; Song, J.-X.; Zhang, M.; Yao, C.; Liu, W.; Huang, M.; Yu, Y.; Yang, Q.; Zhu, T.; Xu, J.; Mu, J.; Wang, Y.; Wang, H.; Tang, T.; Ren, Y.; Wu, Y.; Lin, S.-H.; Qiu, Y.; et al. *Natl. Sci. Rev.* **2020**, *7*, 1157−1168.
(35) Lazari, L. C.; De Rose Ghilardi, F.; Rosa-Fernandes, L.; Assis, D. M.; Nicolau, J. C.; Santiago, V. F.; Dalçóquio, T. F.; Angeli, C. B.; Bertolin, A. J.; Marinho, C. R. F.; Wrenger, C.; Durigon, E. L.; Siciliano, R. F.; Palmisano, G. *medRxiv* **2020**, No. 257006.
(36) Sans, M.; Zhang, J.; Lin, J. Q.; Feider, C. L.; Giese, N.; Breen, M. T.; Sebastian, K.; Liu, J.; Sood, A. K.; Eberlin, L. S. *Clin. Chem.* **2019**, *65*, 674−683.
(37) Zhang, J.; Rector, J.; Lin, J. Q.; Young, J. H.; Sans, M.; Katta, N.; Giese, N.; Yu, W.; Nagi, C.; Suliburk, J.; Liu, J.; Bensussan, A.; DeHoog, R. J.; Garza, K. Y.; Ludolph, B.; Sorace, A. G.; Syed, A.; Zahedivash, A.; Milner, T. E.; Eberlin, L. S. *Sci. Transl. Med.* **2017**, *9*, No. eaan3968.
(38) Pagnotti, V. S.; Chubatyi, N. D.; McEwen, C. N. *Anal. Chem.* **2011**, *83*, 3981−3985.
(39) Kwee, T. C.; Kwee, R. M. *Radiographics* **2020**, *40*, 1848−1865.
(40) Yang, W.; Sirajuddin, A.; Zhang, X.; Liu, G.; Teng, Z.; Zhao, S.; Lu, M. *Eur. Radiol.* **2020**, *30*, 4874−4882.
(41) Ufuk, F.; Savas, R. *Turk. J. Med. Sci.* **2020**, *50*, 664−678.
(42) Xie, X.; Zhong, Z.; Zhao, W.; Zheng, C.; Wang, F.; Liu, J. *Radiology* **2020**, *296*, E41−E45.
(43) Feng, H.; Liu, Y.; Lv, M.; Zhong, J. *Jpn. J. Radiol.* **2020**, *38*, 409−410.
(44) Hossein, H.; Ali, K. M.; Hosseini, M.; Sarveazad, A.; Safari, S.; Yousefifard, M. *Clin. Transl. Imaging* **2020**, 1−13.
(45) Clerici, B.; Muscatello, A.; Bai, F.; Pavanello, D.; Orlandi, M.; Marchetti, G. C.; Castelli, V.; Casazza, G.; Costantino, G.; Podda, G. M. *Front Public Health* **2020**, *8*, No. 593491.
(46) Kucirka, L. M.; Lauer, S. A.; Laeyendecker, O.; Boon, D.; Lessler, J. *Ann. Intern. Med.* **2020**, *173*, 262−267.
(47) He, J. L.; Luo, L.; Luo, Z. D.; Lyu, J. X.; Ng, M. Y.; Shen, X. P.; Wen, Z. *Respir. Med.* **2020**, *168*, No. 105980.

https://doi.org/10.1021/acs.analchem.1c01937
Anal. Chem. XXXX, XXX, XXX−XXX